Optimized Design of Switching Amplifiers for Piezoelectric Actuators

Sriram Chandrasekaran and Douglas K. Lindner

Bradley Department of Electrical and Computer Engineering
Virginia Tech
Blacksburg, VA 24061
(540) 231-4580 (Voice)
(540) 231-3362 (Fax)
lindner@vt.edu

Ralph C. Smith
Center for Research in Scientific Computing
Department of Mathematics
North Carolina State University
Raleigh, NC, 27695

accepted for

Journal of Intelligent Material Systems and Structures
JIMSS-00-040

January, 2001

ABSTRACT

The formulation and solution of an optimization problem for the design of a current controlled switching power amplifier to drive a piezoelectric actuator is the subject of this paper. The design is formulated as a continuous optimization problem. A detailed model that includes the anhysteretic nonlinearity between the electric field and polarization is developed and is coupled with a dynamic model of the amplifier. The design specifications are formulated as optimization constraints. The objective function is chosen to be the weight of the inductor. Optimization results are presented to demonstrate the efficiency of the proposed design methodology.

NOMENCLATURE

Variable	Description
ε_{33}	Dielectric permittivity of piezoelectric actuator material, *farad/meter*
d_{33}	Piezoelectric charge coefficient of actuator, *meter/volt*
Y_{33}	Elastic modulus of actuator, *Newton/meter*^{2}
D_3	Electric displacement or Polarization in actuator, *Coulomb/meter*^{2}
E_3	Electric field in actuator, *Volt/meter*
T_3	Mechanical stress in actuator, *newton/meter*^{2}
S_3	Mechanical strain in actuator
l	Length of actuator, *meter*
w	Width of actuator, *meter*
d	Thickness of a one layer of actuator, *meter*
n	Number of layers
k^2	Electromechanical coupling coefficient
q_l	Charge per layer of the actuator, *coulomb*
C_l	Capacitance per layer of actuator, *farad*
q	Total charge in actuator, *coulomb*
C	Zero stress capacitance of actuator, *farad*
K_1	Strain of actuator/Displacement of structure, *1/meter*
K_2	Force exerted my actuator/Stress in actuator, *1/meter*^{2}
P	Net Polarization in the actuator *C/m*^{2}
P_s	Saturation Polarization of actuator material, *C/m*^{2}
a	Scaling electric field of actuator material, *C/m*^{2}
C_{blk}	Blocked capacitance of actuator, *farad*
V_{m1},V_{m3}, V_{m5}	Fundamental, third and fifth harmonic components of actuator voltage, *volt*
K_a	Equivalent stiffness of actuator, *newton/meter*
M	Mass of structure, *kg*
K	Stiffness of structure, *newton/meter*
B	Damping of structure, n*ewton-sec/meter*
f_{ext}	External disturbance force on structure, *newton*
f_a	Force exerted by actuator on structure, *newton*
v_a	Instantaneous voltage across actuator, *volt*
i_a	Instantaneous current through actuator, *ampere*
$I_{\max}$	Maximum amplitude of actuator current, *ampere*
V_{dc}	DC bus voltage, *volt*
i_{dc}	DC bus current, *ampere*
g_a, g_b	Gating signals to amplifier switches
d_a, d_b	Equivalent duty cycles of g_a, g_b
v_{ab}	Amplifier output voltage, v_{ab}
d_{ab}	Amplifier duty cycle
$d_{ab,\max}$	Maximum amplifier duty cycle
$G_{pq}(s)$	Charge to Polarization transfer function
$G_{pi}(s)$	Current to Polarization transfer function
$H_c(s)$, $H_f(s)$	Current controller transfer functions
ω_F	Excitation frequency of i_{ref}
V_{abk}, I_{ak}, P_k	Harmonic components of amplifier voltage, actuator current and Polarization
I_{dis}	Distortion component of actuator current, *ampere*
THD	Total harmonic distortion of actuator current
K_{1l}, K_{2l}	Aspect ratios of Center leg and window of EE core

C_w, W_w	Widths of center leg and window of EE core, *m*
A_{cp}, A_p	Cross sectional areas of inductor winding and center leg of EE core, m^2
n	Number of turns of inductor winding
l_g	Air gap length of inductor, *m*
μ_o	Permeability of free space, *H/m*
B_{sp}	Saturation flux density of ferrite, *Tesla*
F_w	Window fill factor of EE core
W_{bob}	Width of bobbin of EE core, *m*
F_c	Winding pitch factor of EE core
ρ_{Cu}, ρ_{fe}	Densities of copper and iron, kg/m^3
Vol_{cu}, Vol_{fe}	Volumes of copper in winding and iron in core of inductor, m^3
Z_p	Mean magnetic path length of EE core, *m*
J	Objective function
W_L	Inductor Weight, *kg*
W_{cu}, W_{fe}	Weight of copper and iron in inductor, *kg*
MLT	Mean length/turn of inductor winding, *m*

1. INTRODUCTION

The design of drive amplifiers for piezoelectric and electrostrictive actuators is a challenging task. It is well known that these actuators exhibit highly capacitive electrical characteristics. In addition, these actuators exhibit a hysteretic nonlinearity between the polarization and the electric field. Due to the reactive undamped electrical characteristics of the actuator, the drive amplifier is required to process almost zero real power and a considerable amount of reactive power circulates between the actuator and the amplifier. The size and the weight of the amplifier is determined almost entirely by the amount of reactive power processed. Hence, the amplifier can be large compared to the actuator itself. Therefore, there is interest in determining a minimum weight amplifier for a given actuator. We address this problem herein.

Standard linear amplifiers must dissipate the regenerated energy as heat. These amplifiers automatically require a large heat sink. In contrast, switching amplifiers recycle the regenerative energy back to the power source, resulting in a very efficient amplifier. Because of this property, switching power amplifiers are beginning to be recognized as promising alternatives for driving piezoelectric and electrostrictive actuators (Main, et al., 1995; Zvonar, et al., 1996; Zvonar and Lindner, 1997; Clingman, 1997; Zvonar and Lindner, 1998). In this paper, we focus on an optimization methodology to minimize the weight of a switching amplifier.

Optimization of drive electronics for piezoelectric actuators was addressed by Newton, et al (1996). However, a well-defined optimization procedure that yields physically meaningful designs of the individual components of the amplifier has not been

proposed. To this end, the formulation of an optimization problem for the design of a switching power amplifier to drive a piezoelectric actuator is described. The topology chosen is that of a single-phase DC-AC inverter with a filter inductor connected on the AC side. The switching devices in the amplifier are controlled using the principle of pulse width modulation.

The organization of the paper is as follows: A description of the system under consideration, definition of the design specifications and motivation to optimize the drive amplifier are presented in section 2. A detailed electromechanical model of the piezoelectric actuator coupled to a mechanical structure is developed in section 3. The operating principles of the drive amplifier, pulse width modulation, the development of the average model and implications of using current control are also described in section 3. The determination of the DC bus voltage for the drive amplifier is described in section 4. The estimation of the switching ripple in the actuator current is discussed in section 5. The optimization problem is then explained in detail in section 6. Section 7 consists of the optimization results followed by the conclusions in section 8.

2. PROBLEM DEFINITION

In this paper we consider a switching amplifier driving a piezoelectric actuator attached to a structure as shown in Figure 1. We assume that the piezoelectric actuator and structure are given. In this paper we are interested in the design of the amplifier such that it has minimum weight.

We assume that the amplifier is configured as a current controlled amplifier. That is, the actuator is controlled by controlling the current flowing into the actuator that is proportional to i_{ref}.

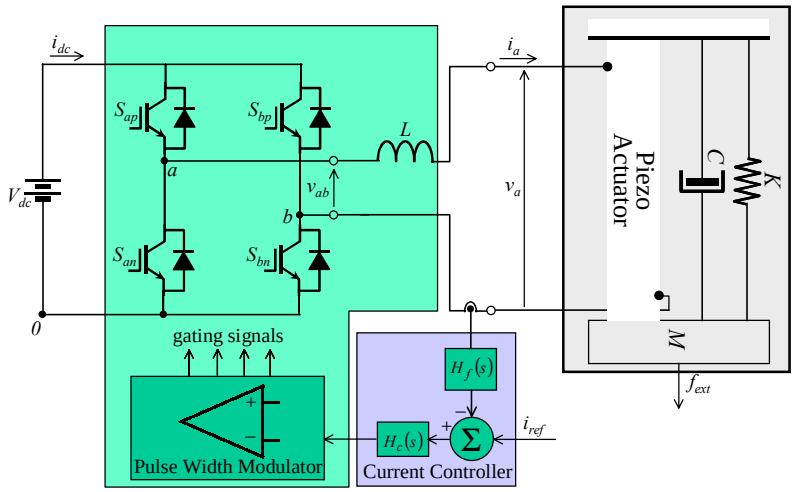

Figure 1. System Under Consideration

(The actuator is not controlled by the voltage across the actuator.) In the frequency domain, this specification is defined in the form of a transfer function shown in Figure 2.

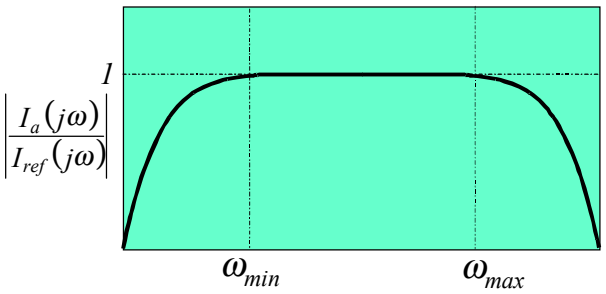

Figure 2. Regulation Specifications of Current Controller

Note that we exclude zero frequency from the passband in this amplifier topology. Clearly, this specification defines the frequency band over which the structure can be

actuated. This data is part of the problem definition including the frequencies ω_{min} and ω_{max}, which define the bandwidth of operation.

We also assume that we want to have the capability to drive the actuator to full stroke over the entire operational frequency range. Since the constitutive equations of the piezoelectric material have a saturation characteristic, this assumption implies that the amplifier must be able to deliver a maximum current over all frequencies in the bandwidth of the amplifier. This maximum current will be calculated below using a nonlinear model of the piezoelectric constitutive equations. This maximum current determines the required value of the bus DC voltage.

The main components of the amplifier are: 1) the switching power transistors with the pulse width modulator, 2) the current controller, and 3) the inductor. The selection of the power transistors is driven by several implementation issues including voltage ratings, thermal dissipation, cost, etc. However, these transistors all tend to be about the same size and weight. Since we are primarily concerned with the performance of the amplifier, we will assume that these switches are ideal, and neglect them in the optimization process.

The current controller is largely driven by the frequency domain requirement on the amplifier given in Figure 2. That is to say, the current controller can be readily determined once the value of the inductance is known. Furthermore, the components of the current controller have a negligible contribution to the weight of the amplifier. Therefore, the current controller is also excluded from the optimization.

In this paper we will focus on the design of the inductor. Indeed, the inductor is by far the largest component over which we have control, and its value is impacted by the other parameters of the amplifier. Here we will consider the actual physical design of the inductor, not only the selection of the inductance value.

The power transistor switches are used to control the average voltage and current that is delivered to the actuator. Due to the switching of these transistors, a ripple voltage and a ripple current ride on top of these average waveforms. This ripple current acts as a disturbance signal on the actuator causing high frequency excitation and unwanted heating in the actuator. The magnitude of the ripple current is determined by the inductor size and the switching frequency of the amplifier. In the optimization process the maximum allowable ripple current is a constraint.

The other component which has a major impact on the weight of the amplifier is the heat sink. The selection of the heat sink depends on the device properties of the transistor switches. Inclusion of thermal considerations is beyond the scope of this paper.

The formulation of the optimization problem consists of the following steps:

1. Modeling the actuator and the amplifier
2. Calculation of the DC bus voltage and current ripple
3. Identification of the design variables
4. Definition of the optimization constraints
5. Definition of the objective function

Each of these steps is described in detail in the following sections.

It is straightforward to formulate the optimization problem. The main challenge is determination of the current ripple. The current ripple can be ascertained from a simulation of the system in Figure 1, which includes the switching dynamics of the

transistors. These simulations, however, are computationally very expensive. Any optimization methodology that includes such a simulation would take prohibitively long to run. Therefore, it is necessary to develop a computationally cheap estimate of the switching ripple. A substantial amount of this paper is devoted to this task.

3. MODEL DEVELOPMENT

Modeling of the Actuator and Structure

The electromechanical model of the piezoelectric actuator coupled to a simple mechanical structure is developed in this section. The linear, constitutive equations of the actuator are used to develop the model. This model can be directly coupled to the dynamic model of the amplifier. Modifications to the linear model to account for the anhysteretic nonlinearity between the polarization and the electric field in the actuator are described. (The anhysteretic nonlinearity arises because of the domain rotations and saturation effects in the piezoelectric material.)

The mechanical model of the actuator-structure is represented by a simple mass-spring-damper system acted on by a disturbance force f_{ext} as shown in Figure 3.

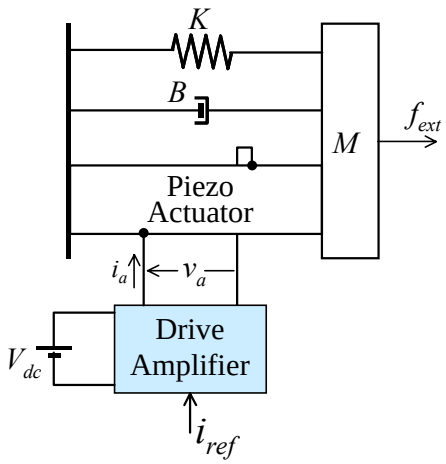

Figure 3. Schematic of amplifier driving the actuator-structure

A drive amplifier operating off a fixed dc voltage V_{dc} provides the power to the piezoelectric actuator. The coordinate system and the forces acting on the mass M are identified in Figure 4 where F_a is the force exerted by the actuator on the mass.

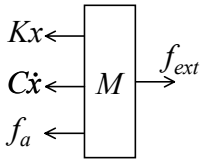

Figure 4. Freebody diagram of the mass

The equation of motion can then be written as

$$M\ddot{x} + B\dot{x} + Kx = f_{ext} - f_a \tag{1}$$

A block diagram representation of Equation (1) is shown in Figure 5.

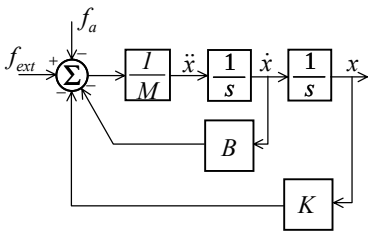

Figure 5. Block diagram representation of structure

The electromechanical model of the actuator is determined in the following. We assume that the actuator has a multilayered stack configuration as shown in Figure 6.

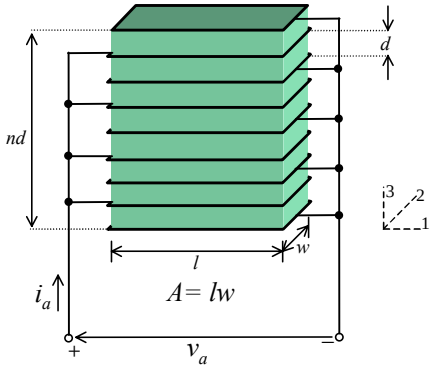

Figure 6. Actuator Configuration

Each layer is rectangular with width w, length l and thickness d. The actuator is formed by stacking n of these layers together. Contiguous layers are polarized in opposite directions and the voltage is applied to the layers as shown in Figure 6. The one-dimensional, linear, coupled, electromechanical, constitutive relations between the strain S_3, stress T_3, electric field E_3, and electric displacement D_3, are

$$D_3 = \varepsilon_{33}^S E_3 + d_{33} T_3 \qquad (2)$$
$$S_3 = d_{33} E_3 + \frac{1}{Y_{33}^E} T_3$$

where, ε_{33} is the dielectric permittivity, Y_{33} is elastic modulus and d_{33} is the transverse piezoelectric charge constant (IEEE Standard on Piezoelectricity). The first index in the

subscripts indicates the direction of the electrical component and the second index indicates the mechanical direction. The superscript indicates that the constant was measured at constant field or strain. (These superscripts are dropped in the subsequent development for simplicity of notation.) The first equation in Equation (2) states that the electric displacement or polarization is the superposition of the direct piezoelectric effect and the applied field times the permittivity. The second equation states that the strain is the superposition of Hooke's law and the converse effect where a mechanical deformation is caused due to the application of an electric field.

Using the geometry of the actuator, we can use Equation (2) to express the relationship between charge and voltage. We assume that the actuator is mechanically unconstrained in the one and two directions. And as usual, the electric field is applied in the three direction. Noting that charge is displacement per unit area, and electric field is voltage per unit length, the charge q_l entering each layer can be obtained as

$$\frac{1}{lw} q_l = \varepsilon_{33} \frac{v_a}{d} + d_{33} T_3 \tag{3}$$

Rewriting this equation we obtain

$$q_l = \varepsilon_{33} \frac{lw}{d} v_a + d_{33} lw = C_l v_a + d_{33} lw T_3 \tag{4}$$

where, C_l represents the capacitance of each layer and v_a is the voltage across the terminals of the actuator. The total charge entering all the n layers of the actuator is then given by

$$q = n q_l = n C_l v_a + d_{33} n lw T_3 \tag{5}$$

Solving Equation (3) for the voltage v_a we obtain

$$v_a = \frac{1}{nC_l} q - \frac{d_{33}}{\varepsilon_{33}} dT_3 = \frac{1}{C} q - \frac{d_{33}}{\varepsilon_{33}} dT_3 \tag{6}$$

where,

$$C = nC_l = \varepsilon_{33}\left(\frac{nlw}{d}\right) \tag{7}$$

From Equation (6) the voltage across a piezoelectric actuator is the resultant of two components: 1) the direct capacitive effect, and 2) a contribution from the mechanical stress. Next we replace electric field by the voltage in the second equation in Equation (2) and substitute in voltage from Equation (6). We obtain

$$\begin{aligned} S_3 &= d_{33}E_3 + \frac{1}{Y_{33}} T_{33} = d_{33}\frac{v_a}{d} + \frac{1}{Y_{33}} T = \frac{d_{33}}{d}\left(\frac{1}{C} q - \frac{d_{33}}{\varepsilon_{33}} dT_3\right) + \frac{1}{Y_{33}} T_3 \\ &= \frac{1}{nlw}\frac{d_{33}}{\varepsilon_{33}} q + \left(1 - k^2\right)\frac{1}{Y_{33}} T_3 \end{aligned} \tag{8}$$

The electromechanical coupling coefficient k^2 is

$$k^2 = \frac{Y_{33} d_{33}^2}{\varepsilon_{33}} \tag{9}$$

This constant is defined as the fraction of the input electrical energy that is mechanically deliverable.

To enter these equations into the block diagram, we rewrite Equation (8) as

$$T_3 = \frac{Y_{33}}{1 - k^2}\left(S_3 - \frac{1}{nlw}\frac{d_{33}}{\varepsilon_{33}} q\right) \tag{10}$$

The block diagram corresponding to these relationships is shown in Figure 7. The displacement in the structure induces a strain in the actuator according to

$$S_3 = K_1 x \tag{11}$$

Similarly, the force applied to the structure by the actuator is derived from the stress in the actuator according to

$$f_a = K_2 T_3 \tag{12}$$

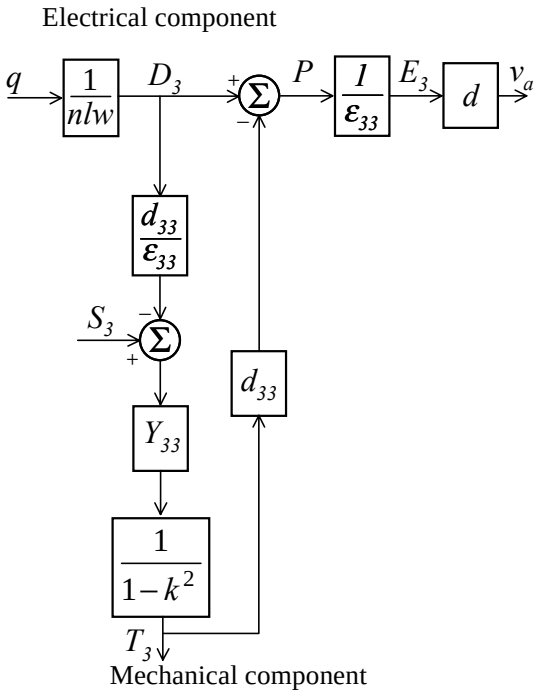

Figure 7. Electromechanical model of piezoelectric actuator

The constants K_1 and K_2 depend on the coupling between the actuator and the structure. They are determined by the location of the actuator, configuration of the actuator, bonding layers, modal coupling coefficients of the structure, and other factors. In general, these constants can be determined using the methods presented by Hagood, et al., (1990), for example. If we interpret the physical system represented by Figure 1 to be a stacked actuator (Figure 6) bonded rigidly to a mass, then the constants K_1 and K_2 are given by

$$K_1 = \frac{1}{nd} \qquad (13)$$
$$K_2 = lw$$

Equations (11) and (12) allow us to couple the actuator equations in Figure 7 to the dynamics of the structure in Figure 5. The complete model is shown in Figure 8.

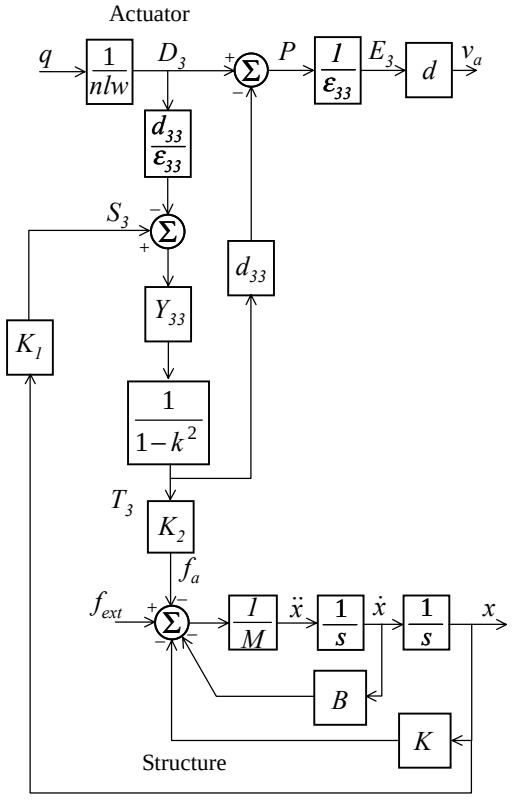

Figure 8. Complete electromechanical model of actuator-structure

The model shown in Figures 7 and 8 has been derived from the linear, coupled constitutive equations (Equation (2)). The modifications in the model to account for the anhysteretic nonlinearity between the polarization and the electric field are described in the following section.

Anhysteretic Nonlinearity

In the absence of interdomain coupling, the anhysteretic nonlinearity according to the Ising spin model between the polarization P, and the electric field E_3, in the actuator is given by Smith and Hom (1999).

$$P = P_s \tanh\left(\frac{E_3}{a}\right) \tag{14}$$

where, P_s is the saturation polarization of the material of the actuator and a is a scaling electric field. However, in the block diagram shown in Figure 8 electric field in the actuator is determined from the polarization. Hence, inverting the nonlinearity given by Equation (14) to conform to the block diagram shown in Figure 8, the electric field is determined as

$$E_3 = a \tanh^{-1}\left(\frac{P}{P_s}\right) \tag{15}$$

This nonlinearity is shown graphically in Figure 9.

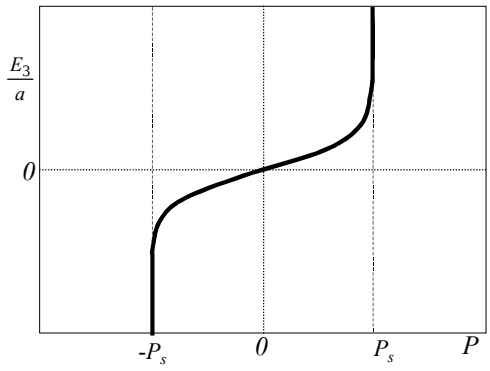

Figure 9. Inverse nonlinearity between polarization and electric field

The block diagram of the electromechanical model of the actuator and the structure with the nonlinearity is shown in Figure 10.

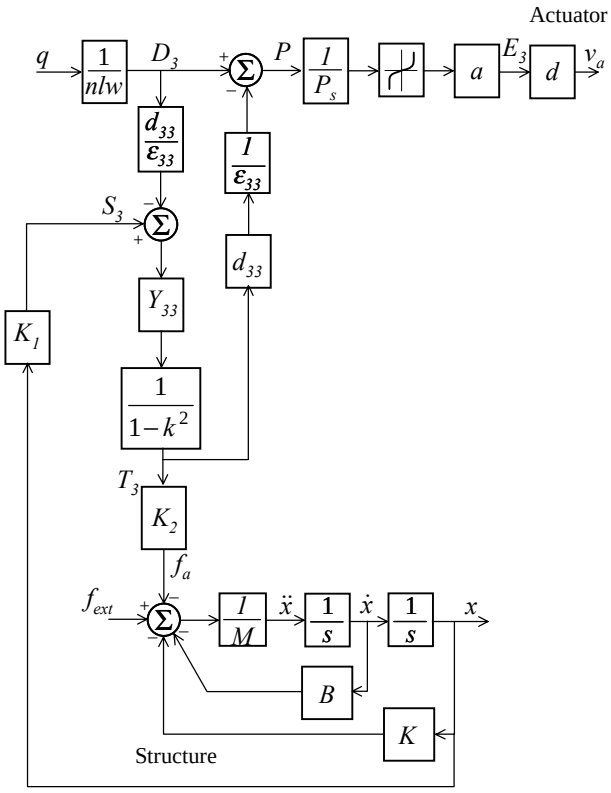

Figure 10. Electromechanical model of actuator-structure with nonlinearity

Under the assumption that the polarization P, does not exceed the saturation polarization P_s a power series expansion can be used to represent the nonlinearity given by Equation (15). This power series expansion for the electric field is given by

$$E_3 = a\left[\left(\frac{P}{P_s}\right)+\frac{1}{3}\left(\frac{P}{P_s}\right)^3+\frac{1}{5}\left(\frac{P}{P_s}\right)^5\right] \tag{16}$$

The actuator model can be represented as a cascade combination of a linear transfer function between the charge and polarization and the nonlinearity between the polarization and the voltage as shown in Figure 11.

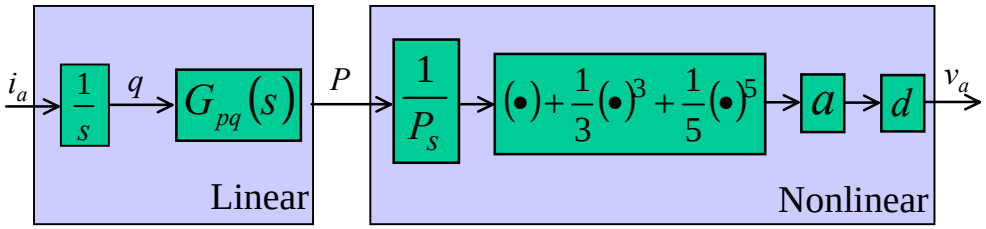

Figure 11. Actuator model as a cascade combination of linear and nonlinear systems

In the following analysis we will frequently use sinusoidal steady state analysis. It is clear from Figure 11 that if the input signal to the nonlinearity is a sinusoid, the output signal will not be purely sinusoidal, but will contain third and fifth harmonics in addition to the fundamental component due to the nonlinearity. Since the actuator current and the polarization are related by a linear transfer function, the polarization is sinusoidal at the same frequency as the actuator current. Hence, if the actuator current is given by

$$i_a(t) = I_{\max}\cos(\omega t) \tag{17}$$

the polarization can be represented as

$$P(t) = P_m\cos(\omega t + \phi) \tag{18}$$

The voltage v_a, at the terminals of the actuator, from Figure 11, is then given by

$$v_a(t) = d\,a\left[\left(\frac{P_m}{P_s}\right)\cos(\omega t+\phi)+\frac{1}{3}\left(\frac{P_m}{P_s}\right)^3\cos^3(\omega t+\phi)+\frac{1}{5}\left(\frac{P_m}{P_s}\right)^5\cos^5(\omega t+\phi)\right] \tag{19}$$

Using trigonometric identities it can be easily shown that v_a consists of the fundamental, third and fifth harmonics and can be expressed as

$$v_a(t) = d\,a\left[V_{m1}\cos(\omega t+\phi)+V_{m3}\cos(3\omega t+3\phi)+V_{m5}\cos(5\omega t+5\phi)\right] \tag{20}$$

where,

$$V_{m1} = \frac{1}{8}\left[8\left(\frac{P_m}{P_s}\right) + 2\left(\frac{P_m}{P_s}\right)^3 + \left(\frac{P_m}{P_s}\right)^5\right] \tag{21}$$

$$V_{m3} = \frac{1}{96}\left[8\left(\frac{P_m}{P_s}\right)^3 + 6\left(\frac{P_m}{P_s}\right)^5\right]$$

$$V_{m5} = \frac{1}{80}\left(\frac{P_m}{P_s}\right)^5$$

Drive Amplifier

Pulse Width Modulation

In this section, we discuss certain aspects of the operation and modeling of the single–phase DC-AC inverter shown in Figure 1. The modulation algorithm and the switching waveform, which it engenders, are briefly discussed. Then a simpler, "average' model of the power stage is introduced. A more detailed description of the power stage and pulse width modulator used in this discussion is shown in Figure 12.

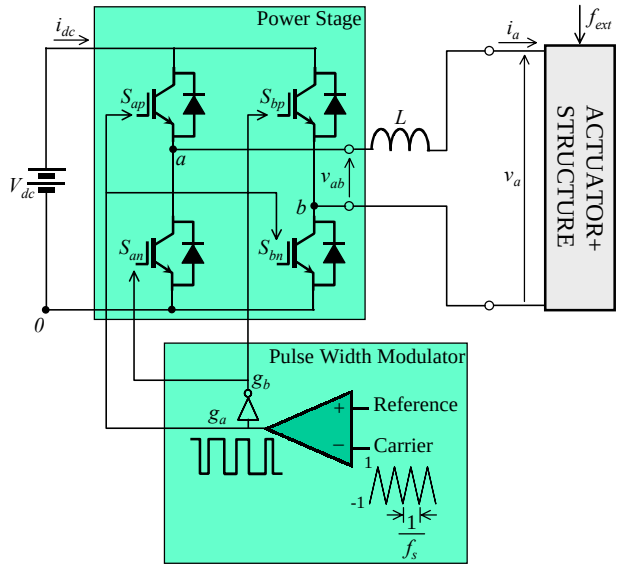

Figure 12. Single phase DC-AC inverter driving the actuator

In this amplifier the current used to drive the piezoelectric actuator is synthesized by pulse width modulating the voltage from the DC source by properly controlling the power transistors with the pulse width modulator. The inductor (in conjunction with the capacitive actuator load) filters the pulse width modulated voltage to deliver a current to the load that contains a fundamental component that is proportional to the reference input signal and that contains an acceptably small current ripple. In order to analyze this current, we begin by analyzing the voltages in the amplifier.

A bipolar voltage v_{ab} is synthesized from the DC voltage source V_{dc} by operating switches S_{ap}, S_{an}, S_{bp} and S_{bn} according to a technique known as pulse width modulation (PWM) (Mohan, et al., 1995). The reference signal is modulated with a triangular wave called the carrier signal as shown in Figure 13. The frequency of the carrier signal is the switching frequency of the amplifier. The signals g_a and g_b are the gating signals generated by the pulse width modulator to drive the four switches of the amplifier. The gating signal g_a, turns on the switches S_{ap} and S_{bn} when the reference signal becomes greater than the carrier signal and turns them off when the reference signal becomes lesser than the carrier. The gating signal g_b, for S_{bp} and S_{an} is the logical inverse of the drive signal to S_{ap} and S_{bn}.

The voltage v_{ab}, shown in Figure 14, at the output of the amplifier is then given by

$$v_{ab} = \begin{cases} V_{dc} & \text{when } S_{ap} \text{ and } S_{bn} \text{ are on} \\ -V_{dc} & \text{when } S_{bp} \text{ and } S_{an} \text{ are on} \end{cases} \qquad (22)$$
$$= g_a V_{dc} - g_b V_{dc}$$

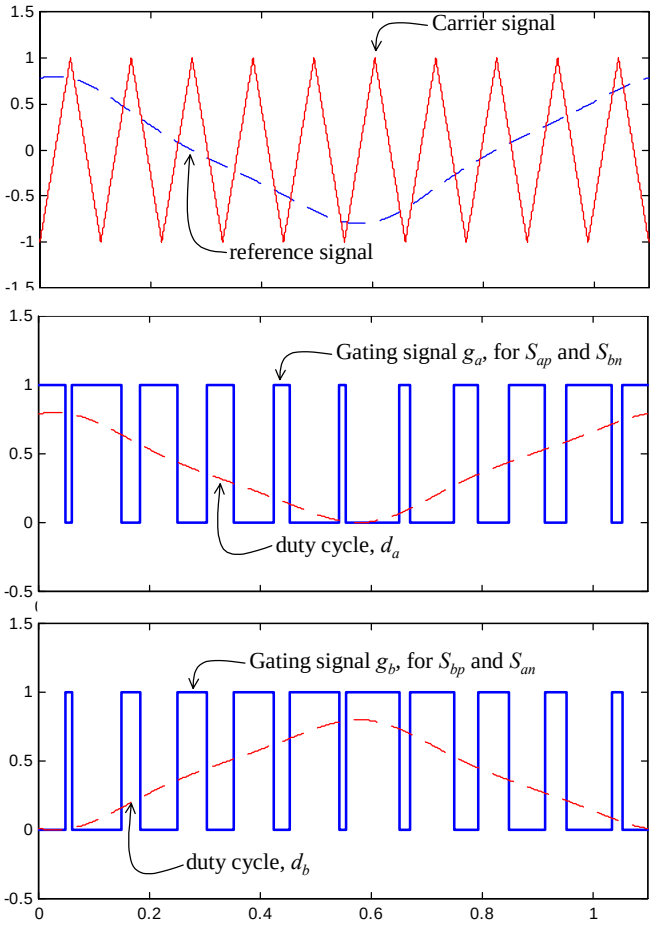

Figure 13. Pulse Width Modulation (PWM)

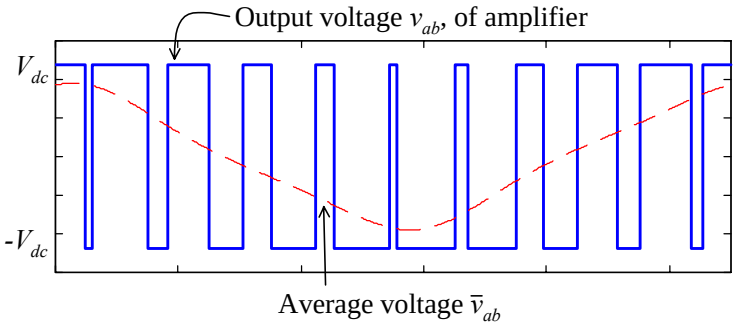

Figure 14. Pulse width modulated voltage v_{ab} and its average value $\bar{v}_{ab}$

The duty cycle of the gating signal is the fraction of the period for which the gating signal is high. The average value of the amplifier output can be obtained from Equation (22) by

replacing the control signals for the switches with the equivalent duty cycles of the gating signals as follows

$$\bar{v}_{ab}(t) = (d_a(t) - d_b(t))V_{dc} = d_{ab}(t)V_{dc} \tag{23}$$

From Equation (23), it can be seen that the duty cycles d_a and d_b can be replaced by a single duty cycle d_{ab} which multiplies the input DC voltage to obtain the average of the output voltage of the amplifier. Since the duty cycle d_{ab} cannot exceed unity, the maximum amplitude of the average value of the output voltage is equal to V_{dc}.

A typical waveform of this actuator current i_a is shown in Figure 15 where it is assumed that the reference input signal is sinusoidal. It can be seen that the actuator current is nearly sinusoidal at the reference frequency. The deviation of the actual current from the desired fundamental component is called the switching ripple.

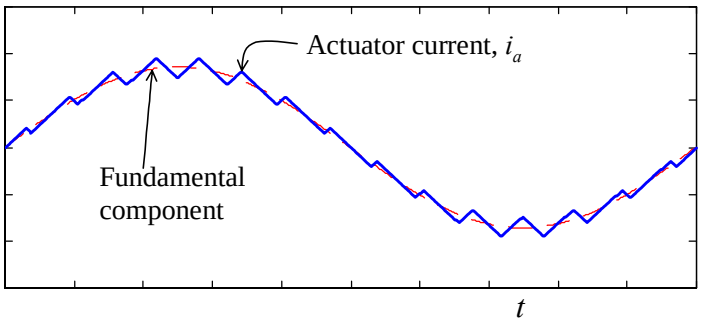

Figure 15. Typical waveform of current generated by the drive amplifier

It can be also shown that the average value of the input current to the amplifier is given by

$$\bar{i}_{dc}(t) = d_{ab}(t)i_a(t) \tag{24}$$

Average Model of Amplifier

In order to incorporate a model of the switching amplifier into the optimization process, it is necessary to replace the switches to make the model computationally tractable. This simplified model, called an average model, neglects the switching ripple in the currents and voltages and reduces the model to a set of relationships between the average waveforms. This model is valid only over frequency ranges significantly lower than half the switching frequency of the amplifier (Kassakian, et al., 1991). The average model is shown in Figure 16.

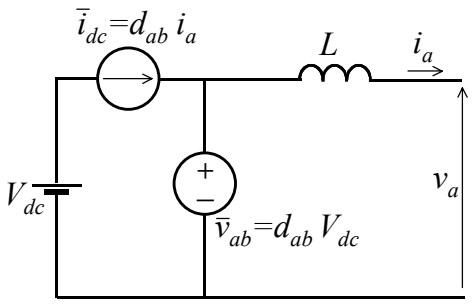

Figure 16. Average model of amplifier driving the actuator

A transfer function representation of the amplifier can be very easily obtained from the average model. A control block diagram representation coupling the models of the amplifier and the actuator is shown in Figure 17.

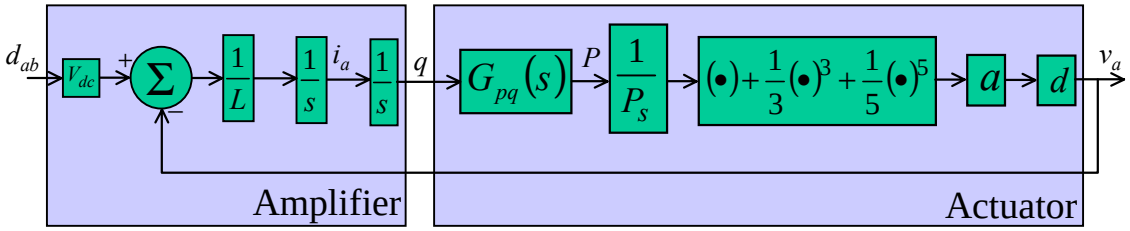

Figure 17. Block diagram of amplifier coupled to the actuator

The final component of the amplifier is the current controller. The block diagram of the closed loop system with a generic representation of the current controller is shown in Figure 18.

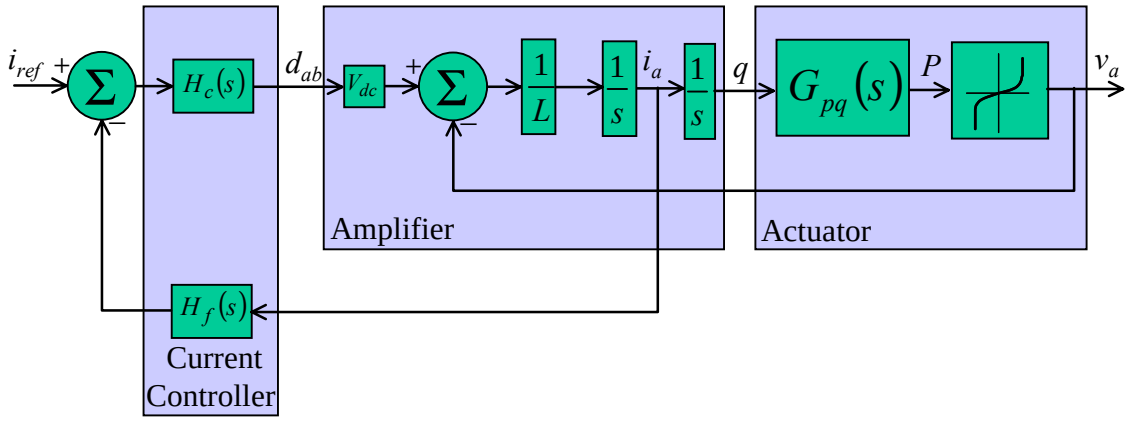

Figure 18. Block diagram of amplifier and actuator with current controller

The current controller ensures that the fundamental component of the actuator current follows the reference over the regulation bandwidth of the amplifier. In the analysis that follows, it is assumed that fundamental component of the actuator current is identical to the reference current command.

This controller uses the current into the actuator as feedback to create an error signal with a reference input signal. The duty cycle command is then synthesized from the error signal. The design of the current controller depends on the inductance L, the capacitance of the actuator, DC input voltage V_{dc} and the switching frequency f_s. The dynamics of the structure can usually be ignored. In this case, the plant to be controlled reduces to a simple second order system. It is a straightforward exercise to design the current controller which turns out to be a proportional or PI controller. In most cases, the current controller can be implemented with analog operational amplifier circuits, whose

weight is negligible compared to the weight of the overall system. Furthermore, the weight of the current controller is independent of the control gains. Therefore, the design of the current controller is excluded from the optimization formulation.

4. DETERMINATION OF DC BUS VOLTAGE

One of the requirements of the amplifier is to drive the actuator to full stroke over the bandwidth of the system. This requirement implies that the amplifier must produce enough current to saturate the piezoelectric actuator when the duty cycle of the amplifier is at its maximum value. This current requirement, in turn, places a restriction on the minimum bus voltage V_{dc}. The minimum bus voltage is related to the inductance, so we need a simple expression for this relationship for the optimization methodology. We use the average model of the amplifier to determine the DC bus voltage neglecting the switching ripple in the actuator current and the voltage. This assumption is validated by the fact that the electromechanical power transfer between the amplifier and the actuator predominantly occurs at the frequency of the reference sinusoidal current, which is much lower than the switching frequency. The determination of the DC bus voltage goes through the following steps. First we determine the maximum current drawn by the actuator. From this current, we determine the voltage across the actuator using the nonlinear model. The amplifier output voltage $\bar{v}_{ab}$, is then calculated as the sum of the actuator voltage and the voltage drop across the inductance. The DC bus voltage is finally determined such that the duty cycle does not exceed unity when $\bar{v}_{ab}$ reaches its maximum amplitude.

A simplified block diagram of the average model of the amplifier and the actuator with the nonlinearity is shown in Figure 19.

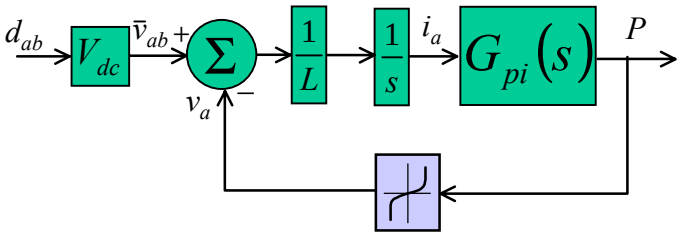

Figure 19. Simplified block diagram of amplifier-actuator with nonlinearity

To start with, we assume that the reference current command is selected to drive the structure at its maximum deflection. This current controlled amplifier is configured such that the fundamental component of the actuator current is identical to the reference current. (See Figure 2). Let this sinusoidal current be given by

$$i_{ref}(t) = I_{\max}\cos(\omega_F t) = i_a(t) \tag{25}$$

where, ω_F is the frequency that results in the maximum deflection. From Figure 19, it can be seen that the actuator current and polarization are linearly related by a transfer function $G_{pi}(j\omega)$, whose magnitude response is shown in Figure 20.

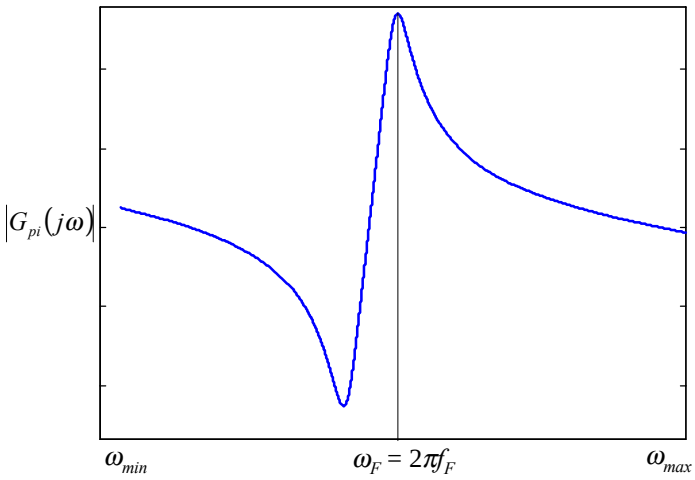

Figure 20. Actuator current to polarization transfer function

(In this case, the amplifier bandwidth is assumed to include the mechanical resonant frequency of the structure. For this particular example, ω_F is the damped resonance of the structure.) Hence, for the actuator current given by (25), the polarization can be expressed as

$$P(t) = P_s \cos(\omega_F t + \phi) \tag{26}$$

since the actuator is being driven to its maximum deflection. Using the relationship in Figure 20 between the current and polarization, we immediately have

$$I_{\max} = \frac{P_s}{G_{PI}(j\omega_F)} \tag{27}$$

The next step is to determine the voltage across the actuator using the nonlinear constitutive equations of the piezoelectric material. Given the polarization in (26) the actuator voltage consists of the fundamental, third and fifth harmonics according to Equations (19), (20) and (21) because of the nonlinearity. Substituting $P_m = P_s$ in (21), we obtain

$$v_a(t) = d\,a\left[\frac{11}{8}\cos(\omega_F t+\phi)+\frac{7}{48}\cos(3\omega_F t+3\phi)+\frac{1}{80}\cos(5\omega_F t+5\phi)\right] \tag{28}$$

From Figure 16, the voltage $\bar{v}_{ab}$, at the output of the amplifier is the sum of the actuator voltage and the drop across the inductor. This voltage is given by

$$\bar{v}_{ab}(t) = L\frac{di_a(t)}{dt}+v_a(t) \tag{29}$$

Substituting for $i_a(t)$ from Equation (25) and for $v_a(t)$ from Equation (28), we obtain

$$\bar{v}_{ab}(t) = d\,a\left[\frac{11}{8}\cos(\omega_F t+\phi)+\frac{7}{48}\cos(3\omega_F t+3\phi)+\frac{1}{80}\cos(5\omega_F t+5\phi)\right] + \omega L I_{\max}\sin(\omega_F t) \tag{30}$$

It can be seen from Equation (29) that, in order to guarantee the sinusoidal actuator current given by Equation (25), the current controller (Figure 19) needs to synthesize a duty cycle command d_{ab}, such that the third and fifth harmonic components of the amplifier output voltage $\bar{v}_{ab}$ are identical to those of the actuator voltage v_a. According to Equation (23), the duty cycle $d_{ab}(t)$ can be written as

$$d_{ab}(t) = \frac{1}{V_{dc}}\bar{v}_{ab}(t) \tag{31}$$

The minimum DC bus voltage required is then determined such that the duty cycle given by Equation (31) does not exceed its maximum allowable amplitude $d_{ab,\max}$ when the amplifier output voltage $\bar{v}_{ab}$, reaches its maximum amplitude. The minimum DC bus voltage is hence obtained as

$$V_{dc} = \frac{1}{d_{ab,\max}}\max[\bar{v}_{ab}(t)] \tag{32}$$

5. ESTIMATION OF ACTUATOR CURRENT

The next step in the analysis is to determine the current ripple. Specifications on the harmonic content of the actuator current are used as optimization constraints to determine the values of inductance and switching frequency. This analysis is complicated by the nonlinear constitutive equations of the actuator. One approach for determining the current ripple is to directly simulate the nonlinear system. This method is computationally too expensive for optimization, however. Therefore, we will estimate the size of the current ripple by computing the amplitudes of the components of the Fourier series of the actuator current.

The switching of the power transistors causes the voltage v_{ab} in Figure 14 to be a pulse width modulated square wave. We determine a Fourier decomposition of the voltage v_{ab} given by,

$$v_{ab}(t) = \sum_{k=1}^{\infty} V_{abk} \cos(\omega_k t + \vartheta_k) \tag{33}$$

A typical harmonic spectrum of the amplifier output voltage is shown in Figure 21.

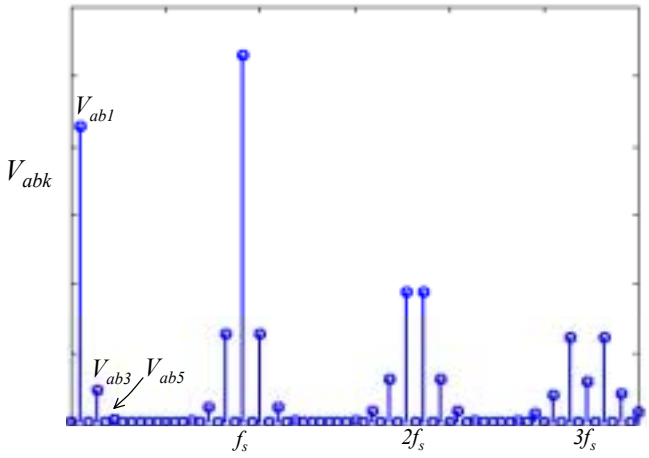

Figure 21. Harmonic spectrum of amplifier output voltage v_{ab}

The first, third and the fifth harmonics of the voltage v_{ab}, are given by Equation (30). Since the actuator current has no third and fifth harmonics, the third and fifth harmonic components of amplifier output voltage are identical to those of the actuator voltage v_a and do not contribute to the ripple in the actuator current. The distortion in the actuator current is due to the voltage harmonics whose frequencies are in the switching frequency range.

The Fourier decomposition of the actuator current can be expressed as

$$i_a(t) = I_{\max}\cos(\omega_F t) + \sum_{k=2}^{\infty} I_{ak}\cos(\omega_k t + \theta_k) \tag{34}$$

It is assumed that the fundamental component of the actuator current i_a is identical to i_{ref}. The polarization and actuator voltage can also be expressed in a similar fashion as

$$P(t) = P_s\cos(\omega_F t + \phi) + \sum_{k=2}^{\infty} P_k\cos(\omega_k t + \phi_k) \tag{35}$$

$$v_a(t) = \sum_{k=1}^{\infty} V_{ak}\cos(\omega_k t + \varphi_k)$$

The harmonic components of v_a for k=1,3 and 5 are given by Equation (28). We use complex phasor notation of sinusoidal steady state variables to determine the Fourier components of the actuator current. Rewriting Equation (29) in complex phasor notation we obtain

$$V_{abk}e^{j\vartheta_k} = V_{ak}e^{j\varphi_k} + \omega_k L I_{ak}e^{j\left(\theta_k + \frac{\pi}{2}\right)} \tag{36}$$

The amplitudes I_{ak}, of the actuator current are then obtained from Equation (36) as

$$I_{ak} = \frac{1}{\omega_k L}\left(V_{abk}e^{j\left(\vartheta_k - \theta_k - \frac{\pi}{2}\right)} - V_{ak}e^{j\left(\varphi_k - \theta_k - \frac{\pi}{2}\right)}\right) \tag{37}$$

To obtain the Fourier series components of the actuator current, the corresponding components of the actuator voltage are required according to Equation (37). Typical switching waveforms of the actuator current, actuator voltage and amplifier output voltage are shown in Figure 22.

From Figure 22 it can be seen that the polarization and the actuator voltage are distorted with negligible switching ripple. The reasons for this are explained in the following. An expanded view of magnitude of the transfer function $G_{pi}(s)$, from the actuator current to the polarization is shown in Figure 23.

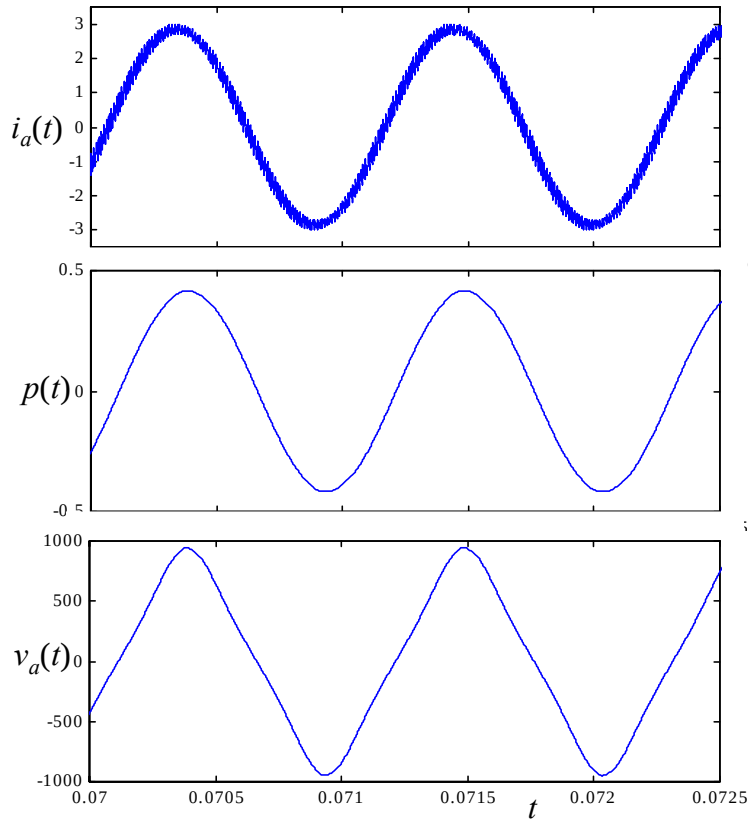

Figure 22. Switching waveforms of actuator current i_a, duty cycle d_{ab}, and actuator voltage v_a.

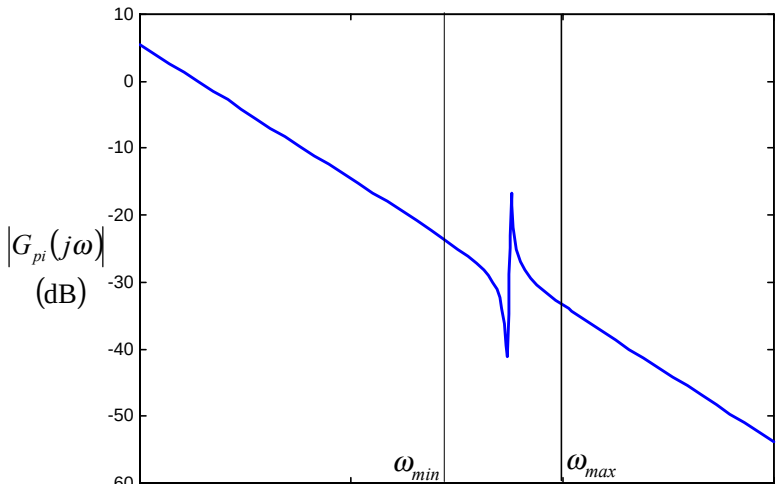

Figure 23. Expanded of transfer function $G_{pi}(s)$ from actuator current to polarization

Since the switching frequency has to be significantly higher than ω_{max}, it can be seen from Figure 23, that harmonics of the current in the switching frequency range are sufficiently attenuated by the transfer function $G_{pi}(s)$. Hence, it can be assumed that the harmonic components at the switching frequency range of the polarization are equal to zero. In addition, due to the static nonlinearity between the polarization and the electric field, the actuator voltage can also be assumed to be devoid of any components in the switching frequency range. As a result, we have

$$P_k = 0 \text{ for } k \geq 2$$
$$V_{ak} = 0 \text{ for } k \geq 6 \tag{38}$$

Hence, Equation (37) reduces to

$$I_{ak} = \frac{1}{\omega_k L} V_{abk} \text{ for } k \geq 6 \tag{39}$$

6. FORMULATION OF OPTIMIZATION PROBLEM

Introduction

We are now ready to establish the optimization methodology using the calculations in the previous sections. We will proceed by identifying the design variables, setting up the constraints, and defining the objective function.

Design Variables

The design variables for the optimization problem are the variables associated with the design of the inductor. The inductor design includes the physical design of the inductor's components, not just the selection of the value of the inductance. The inductors are assumed to be typical EE cores as shown in Figure 24.

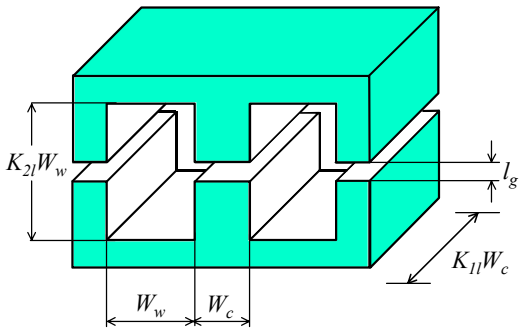

Figure 24. EE Core and relevant dimensions

The bobbin is housed on the center leg of the core as shown in Figure 25.

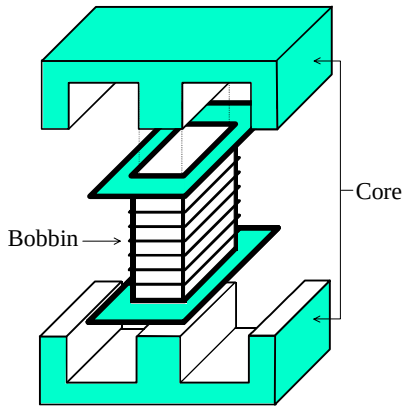

Figure 25. Exploded inductor core and bobbin assembly

The quantities K_{1l} and K_{2l} shown in Figure 24 are assumed to be fixed and represent the aspect ratios of the center leg and the window, respectively (Ridley, et al., 1990). The design variables are listed in Table 1. The design variables include parameters related to the windings and wire size.

Table 1. Design variables associated with inductor design

Variable name	Description
n	Number of turns
A_{cp}	Cross sectional area of winding
C_w	Center leg width
W_w	Window width
l_g	Airgap length

The inductance as a function of the physical variables is given by

$$L = \frac{\mu_o K_{1l} C_w^2 n^2}{l_g} \tag{40}$$

Constraints

The optimization constraints are subdivided into performance and physical constraints as explained in the following subsections.

Performance Constraints

Total Harmonic Distortion of Actuator Current

The first performance constraint is the maximum allowable current ripple. Because the current ripple is a nonlinear function, we express the actuator current as a Fourier series Equation (34), and then measure the current ripple as total harmonic distortion. The *THD* is the percentage ratio of the distortion component of the actuator current to its fundamental component (Mohan, et al., 1995). It is defined as

$$THD = 100\frac{I_{dis}}{I_{a1}} \tag{41}$$

where, I_{a1} is the rms value of the fundamental component of the actuator current and I_{dis} is the rms value of the distortion component. The fundamental component of the actuator current is assumed to be identical to the reference command. According to Equation (34), the distortion component is given by

$$I_{dis} = \sum_{h=2}^{\infty}\frac{I_{ak}^2}{2} \tag{42}$$

The *THD* of the amplifier used at full capacity can be expressed as

$$THD = 100\sqrt{\frac{\sum_{k=2}^{\infty} I_{ak}^2}{I_{\max}^2}} \tag{43}$$

An upper bound is imposed on the *THD* of the actuator current to size the inductor at the specified switching frequency.

The *THD* of the actuator current is a function of the switching frequency and the amplitude and the frequency of the fundamental component of the actuator current. To begin with, the switching frequency is fixed at a specified value. The amplitude and frequency of the fundamental component of the actuator current are determined from the

mechanical model according to Equation (27) and Figure 20. The average amplifier output voltage $\bar{v}_{ab}$ then is determined for this maximum current amplitude from Equation (30). The DC bus voltage is then determined from Equation (32) using the maximum duty cycle. For this DC bus voltage the duty cycle d_{ab}, is determined from Equation (31). This duty cycle is then modulated with the triangular carrier at the switching frequency as shown in Figure 13 to generate the pulse width modulated output voltage v_{ab} as shown in Figure 14. The Fourier components V_{abk}, of the pulse width modulated voltage v_{ab} are then determined. Finally, the Fourier series components of the actuator current are determined from Equation (39) where the inductance is determined from Equation (40). The *THD* of the actuator current is then determined from Equation (43).

Physical Constraints

Physical constraints are defined to guarantee physically meaningful dimensions for the core and windings used in the inductor (Figure 24). They are defined as follows:

- The widths of the center leg C_w, and of the window W_w are not allowed to be less that 1 mm to ensure sufficient mechanical strength of the core.

- In order to ensure sufficient mechanical strength for the winding, the copper wire used cannot be greater than 30AWG, which is equivalent to a cross-sectional area of 7.29×10^{-8} m^2.

- The number of turns in the inductor cannot be less than one and must be an integer.

- The current density in the windings of the inductor cannot be greater than maximum allowable current density for copper.

$$\frac{I_a}{A_{cp}} < J_{Cu} = 1.5 \times 10^6 \text{ A/m}^2 \tag{44}$$

- The available window area of the EE core must be large enough to accommodate the windings of the inductor and the bobbin, which houses the windings (Figure 22).

$$K_{2l} W_w^2 > \left(\frac{nA_{cp}}{F_w} + W_{bob} K_{2l} W_w \right) \tag{45}$$

where,

$$\begin{aligned} F_w &= 0.4 \\ W_{bob} &= 1.5 \text{ mm} \\ K_{2l} &= 3 \end{aligned} \tag{46}$$

- The dimensions of the inductor should be such that the maximum allowable saturation flux density for core material (which is assumed to be ferrite) is not exceeded according to

$$B_{sp} > \frac{LI_{\max}}{nK_{1l} C_w^2} \tag{47}$$

Objective Function

The objective function *J*, is the weight of the inductor. That is,

$$J = W_L \tag{48}$$

The weight of an inductor is determined as the sum of the weights of iron and copper used in the core and windings, respectively

$$W_L = W_{fe} + W_{cu} \tag{49}$$

From Figure 22, the weight of the copper can be obtained as

$$W_{cu} = D_{cu} Vol_{cu} \tag{50}$$

where,

$$\begin{aligned} &\rho_{cu} = 8900 \text{kg/m}^3 \\ &Vol_{cu} = MLT \cdot n \cdot A_{cp} \\ &MLT = 2F_c C_w (1 + K_{1l}) \\ &F_c = 1.9 \end{aligned} \tag{51}$$

Similarly the weight of the iron used in the EE core is given by (Figure 24)

$$W_{fe} = D_{fe} Vol_{fe} \tag{52}$$

where,

$$\begin{aligned} &\rho_{fe} = 7800 \text{kg/m}^3 \\ &Vol_{fe} = Z_p A_p \\ &Z_p = 2(1 + K_{2l}) W_w + \frac{\pi}{2} C_w \\ &A_p = K_1 C_w^2 \end{aligned} \tag{53}$$

7. OPTIMIZATION RESULTS

The results of the optimization problem are presented in this section. The bandwidth requirements and relevant specifications of the actuator are given below in Table 2.

Table 2. Operating Conditions

Variable	Value
Operating bandwidth	$\omega_{min} = 2\pi$ 700 rad/sec < ω < $\omega_{max} = 2\pi$ 1200 rad/sec
Dielectric Permittivity, ε_{33}	(1800)(8.854 x 10^{-12}) F/m
Piezoelectric Coefficient, d_{33}	3.8568 x 10^{-10} m/V
Elastic Modulus, Y_{33}	5.5×10^{10} F/m
Actuator Length, l	0.01 m
Actuator Width, w	0.01 m

Layer Thickness, d	0.0001 m
Saturation Polarization, P_s	0.425 C/m^2
Coercive Electric Field, a	6.4 MV/m
Mass of Structure, M	200 kg
Damping of Structure, B	2.56 x 10^4 N-s/m
Stiffness of Structure, K	5.4 x 10^9 N/m
V_{dc}	1186 V (determined from (32))
$I_{\max}$	2.8895 A (determined from (27))

Optimization was performed using the VisualDOC optimization software (Vanderplaats, 1988) using the Modified Method of Feasible Directions algorithm (Haftka and Gürdal, 1992). The optimization algorithm used for the present work belongs to a class of optimization algorithms termed "gradient based methods". If the design space contains several local minima, there is a possibility that a gradient-based optimizer may be trapped by a local minimum, and the answer will depend on the selection of the initial design point. In the present work, it was found that there were not any local minima in the design space, and the optimizer converged to the global minima irrespective of the choice of the initial design. The optimizations were achieved in approximately 10 minutes on a 500 MHz Pentium III PC.

A family of optimal designs was obtained by varying the upper bound on the THD of the actuator current for switching frequencies of 100 kHz and 200 kHz. The inductance values plotted as a function of the THD of the actuator current for the two values of switching frequency is shown in Figure 26. It can be seen that the inductance increases as the upper bound on the THD decreases for a given switching frequency. In addition, the inductance value required to meet a given THD specification reduces as the switching frequency increases.

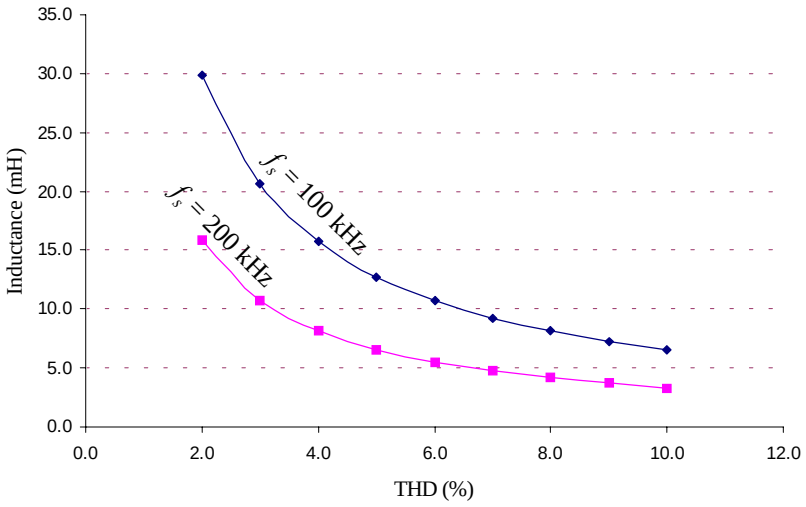

Figure 26. Inductance value *vs* THD of actuator current

The weight of the inductor as a function of the inductance value is plotted in Figure 27.

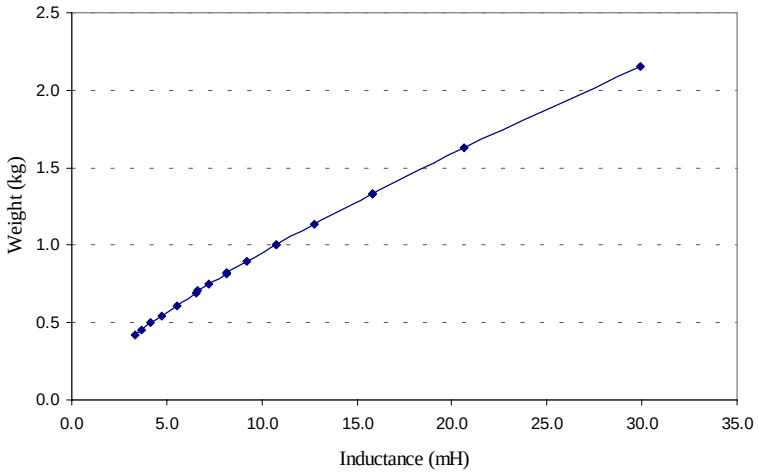

Figure 27. Weight of the inductor *vs* inductance value

The weight of an inductor is proportional to the energy stored, which in turn is proportional to inductance value and to the square of the peak inductor current. Since the peak current is approximately constant (determined by the maximum polarization), the weight of the inductance varies almost linearly with inductance.

8. CONCLUSIONS

In this paper we discuss the problem of designing a minimum weight, current controlled switching amplifier for a piezoelectric actuator. These results are partial in that the design of the heat sink is ignored. With this assumption the design of the amplifier reduces to the design of the inductor. Indeed, the inductor is the largest single component of the amplifier. An optimization methodology is formulated that takes into account the physical configuration of the inductor, the bandwidth of the amplifier, the effect of the ripple current and switching frequency on the sizing of the inductor. The optimization results demonstrate that the proposed optimization formulation provides an effective method to obtain physically meaningful results in a time efficient manner.

ACKNOWLEDGEMENTS

The research reported in this paper is supported by the AFOSR under grant numbers F49620-97-1-0254 and made use of ERC Shared Facilities supported by the National Science Foundation under Award Number EEC-9731677.

REFERENCES

1. Zvonar, G. A. and D. K. Lindner, 1998 "Power Flow Analysis of Electrostrictive Actuators Driven by Switchmode Amplifiers," *Journal on Intelligent Material Systems and Structures,* special *issue on the 3rd Annual ARO Workshop on Smart Structures*, Vol. 9, No 3, pp. 210 - 222.
2. Zvonar, G. A. and D. K. Lindner, "Nonlinear Electronic Control of an Electrostrictive Actuator," *Proceeding of SPIE's 1997 North American Symposium on Smart Structures and Materials: Industrial and Commercial Applications of Smart Structures Technologies*, Janet M. Sater; Ed., Vol. 3044, San Diego, CA, March, 1997, pp. 448-458.
3. Clingman, J. D. "Drive Electronics for Large Piezoactuators," *Proceeding of SPIE's 1997 North American Symposium on Smart Structures and Materials: Industrial and Commercial Applications of Smart Structures Technologies*, Janet M. Sater; Ed., Vol. 3044, San Diego, CA, March, 1997, pp. 459-467.
4. Zvonar, G. A., J. Luan, F. C. Lee, D. K. Lindner, S. Kelly, D. Sable, and T. Schelling, "High-Frequency Switching Amplifiers For Electrostrictive Actuators", *Proceedings of SPIE's 1996 North American Symposium on Smart Structures and*

Materials: Industrial and Commercial Applications of Smart Structures Technologies, C. Robert Crowe; Ed., Vol. 2721, San Diego, CA, February, 1996, pp. 465-475.

5. Main, J.A, E. Garcia, and D.V Newton, "Precision Position Control of Piezoelectric Actuators using Charge Feedback," *Journal of Guidance, Control and Dynamics*, Vol. 18, No. 5, Sep-Oct 1995, pp. 1068-1073.
6. Newton, D.V, J. A. Main, E. Garcia, and L. Massengill, "Piezoelectric Actuation Systems: Optimization of Driving Electronics," *Proceedings of SPIE's 1996 North American Symposium on Smart Structures and Materials: Smart Structures and Integrated Systems*, Vol. 2717, San Diego, CA, February 1996, pp. 259-266.
7. Smith R.C, and C.L. Hom,. "A Domain Wall Model for Ferroelectric Hysteresis", *Proceedings of SPIE, The International Society for Optical Engineering,* Vol.3667, 1999, pp.150-61. USA.
8. Mohan N., T.M. Undeland, and W. Robbins, *Power Electronics-Converters, Applications and Design*, John Wiley and Sons, 1995.
9. Kassakian J.G, M.F. Schlecht, and G.C. Verghese, *Principles of Power Electronics*, Addison-Wesley, 1991.
10. Ridley R.B., C. Zhou, and F.C. Lee, "Application of Nonlinear Design Optimization for Power Converter Components", *IEEE Transactions on Power Electronics*, vol. 5. no. 1., January 1990, pp. 29-39.
11. Vanderplaats, G.N., *Numerical Optimization Techniques for Engineering Design: With Applications*, Vanderplaats R&D Inc., Colorado Springs, CO, 1988.
12. Haftka, R.T and Z. Gürdal, *Elements of Structural Optimization, Third Revised and Expanded Edition*, Kluwer Academic Publishers, Dordrecht, 1992, pp. 182-186.
13. Hagood, N. W., W. H. Chung, and A. von Flotow, "Modeling of Piezoelectric Actuator Dynamics for Active Structural Control," *Journal on Intelligent Material Systems and Structures,* Vol. 1, No. 3, July, 1990, pp. 327 – 354.
14. IEEE Standard on Piezoelectricity, 1988.